

Revisiting the Properties of Edge-Bridged Bromide Tantalum Clusters in the Solid-State and in Solution and vice-versa: An Intertwined Experimental and Modelling Approach

Maxence Wilmet, Clément Lebastard, Flavien Sciortino, Clothilde Comby-Zerbino, Luke MacAleese, Fabien Chirot, Philippe Dugourd, Fabien Grasset, Yoshitaka Matsushita, Tetsuo Uchikoshi, Katsuhiko Ariga, Pierric Lemoine, Adèle Renaud, Karine Costuas, Stéphane Cordier

SUPPORTING INFORMATION

I. Experimental Section

Experimental procedures	S2
Figure S1. XRPD Le Bail refinement of 1	S6
Figure S2. XRPD Rietveld refinement of 2_γ	S6
Table S1. Refined atomic coordinates of 2_γ .	S6
Table S2. Interatomic distances deduced from Rietveld refinement of XRD data	S7
Figure S3. XRPD Rietveld refinement of 2_β	S8
Figure S4. Thermal gravimetric analysis (TGA) of 2_α and 2_β	S8
Figure S5. Comparison of XRPD patterns of 2_α and 2_β at 25°C and 400°C	S9
Figure S6. Evolution of the XRPD patterns of 2_α and 2_β between 25°C and 400°C	S10
Figure S7. Normalized Raman spectra of 2_δ compared with those of 2_α , 2_β	S11
Figure S8. Normalized UV-visible spectra of 1 in different solvents	S11
Figure S9. Normalized UV-visible spectra of 1 in water + SnBr ₂ and Fe(NO ₃) ₃	S11

II. Computational study

Computational details	S13
Tables S3. Cartesian coordinates of the optimized geometries and	S14
Figure S10. Simulated Raman spectra of [$\{\text{Ta}_6\text{Br}_{12}\}\text{Br}_6^{\text{a}}$] ⁴⁻	S17
Table S4. TD-DFT vertical electronic singlet-singlet excitations	S17
References	S21

Experimental procedures

*Synthesis of crude $K_4[\{Ta_6Br^{i}_{12}\}Br^a_6]$ (**1**).* **1** was prepared following a procedure recently described on the basis of early work of the group of McCarley.¹ $K_4[\{Ta_6Br^{i}_{12}\}Br^a_6]$ is obtained by the reduction of tantalum pentabromide ($TaBr_5$) powder by tantalum powder in an alkaline medium (KBr) at high temperature under an inert atmosphere. The relative proportion KBr: $TaBr_5$:Ta in this synthesis is 4:14/5:4. Thus, 1.720 g of $TaBr_5$ (2.97 mmol, Alfa Aesar, 99.9% (metals basis)), 0.769 g of Ta (4.25 mmol, Alfa Aesar-325 mesh, Puratronics, 99.97% (metals basis)) and 0.498 g of KBr (4.25 mmol, Acros Organics, > 99% (ACS reagent)) were mixed together in a glovebox (Ar atmosphere), put into a silica tube and sealed under vacuum. The $K_4[\{Ta_6Br^{i}_{12}\}Br^a_6]$ phase was obtained after a heating treatment at 650°C for 24 hours in a rocking furnace. X-Ray powder diffraction analysis of the resulting powder (Fig. S1) revealed the presence of $K_4[\{Ta_6Br^{i}_{12}\}Br^a_6]$ along with an excess of tantalum powder and KBr. This as-prepared powder sample is named **1** thereafter in the text. Dissolution of **1** in solvents deserves to measure the amount of by-products (in particular unreacted KBr and Ta) thanks to the difference in solubility between those by-products and $K_4[\{Ta_6Br^{i}_{12}\}Br^a_6]$. To do so, 1 g of **1** was dissolved under argon atmosphere in dried acetone, in which, Ta (metallic form), KBr, and traces of amorphous inorganic species are hardly soluble. This remaining solid product was recovered, dried and weighted. It corresponds to 33.7 ± 0.5 % by weight of **1** and consequently **1** contains 66.3 ± 0.5 % of $K_4[\{Ta_6Br^{i}_{12}\}Br^a_6]$. This acetone insoluble powder was recovered and then poured in water in order to estimate the percentage of water-soluble by-products (KBr and amorphous). The remaining undissolved compound was recovered, dried, weighted and analysed. It corresponds to tantalum powder and represents 12.7 ± 0.5 % by weight of **1**. Therefore, the soluble impurities in water correspond to 21.0 ± 0.5 % of **1**. These experiments were made several times for different batches of **1** prepared in the same experimental conditions and they are reproducible. To conclude, **1** contains in weight %: 66.3 ± 0.5 % of

$K_4[\{Ta_6Br^{12}\}Br^a_6]$, 12.7 ± 0.5 % of Ta and 21.0 ± 0.5 % of KBr and amorphous water-soluble by-products. It has to be noted that the error bar of 0.5% considers the error on the weight measurements as well as partial dissolution of KBr in acetone in minor amount.

Synthesis of $2_\alpha - Ta_6Br_{14} - 14 H_2O$. The compound 2_α was obtained by the simple dissolution of **1** in water, filtration and recrystallization by evaporation in ambient conditions. 100 mg of **1** were added in 5 ml of water. Then, after filtration, the solution was let to evaporate in air. Contrarily to the preparation of 2_β described just below on the basis of a synthesis initially reported by Koknat,³⁵ this experimental protocol does not involve any acid. The obtain powder contains KBr impurities (21.0 ± 0.5 %).

Synthesis of $2_\beta - Ta_6Br_{14} - 8 H_2O$. – A protocol derived from that of Messerle and coworkers and McCarley and coworkers was developed.^{1c,2} 1.5 g of **1** were introduced in 10 ml of degassed water under argon. After 10 hours of stirring, the solution was decanted and filtered under a flux of argon. Then, 225 mg of $SnBr_2$ were dissolved in air in 5 ml of concentrated HBr (ACROS OrganicsTM, 48 wt. % solution in water). After full dissolution, the latter solution was added to the solution of **1**. Afterwards, this solution was slowly heated to 80°C in air under stirring. Heating was stopped after 45 min. A second acidic solution was added and the solution was let to cool down. When the temperature of 30°C was reached, a third acidic solution was added and the beaker was put in ice. Microcrystalline powder was recovered after filtration on a glass frit. The powder was then washed with HBr and ether and dried over P_2O_5 ; yield 0.75 g, 86% subtracting **1** impurities. EDS analysis of heavy elements *i.e.* Br and Ta for selected crystals from the preparation revealed an average atomic composition of 70% for bromine and 30% for Ta in full agreement with the theoretical one for Ta_6Br_{14} (30:70).

Synthesis of $2_\gamma - Ta_6Br_{14} - 7 H_2O$. 100 mg of **1** were dissolved in 15 mL of acetone and stirred for 24 hours. Then, the solution was centrifuged and supernatant was collected. 200 μ L of this solution was poured in a vial. Then, 800 μ L of a 1 μ M solution of cetyltrimethylammonium

chloride was added and the mixture vigorously vortexed. The suspension was let to rest and crystalline sediment powder were obtained within 10 h.

*Synthesis of $(TBA)_2[\{Ta_6Br^{i}_{12}\}Br^a_6]$ **3*** – 100 mg of **1** were put in 5 mL of acetone and stirred 24 hours under air. The resulting brown solution was filtered. 0.009 g ($2.72 \cdot 10^{-5}$ mol) of $(TBA)Br$ ($TBA^+ = [N(C_4H_9)_4]^+$) were added to 2 mL of this solution. The solution was stirred 24 hours under air. The solvent was then evaporated. $(TBA)_2[\{Ta_6Br^{i}_{12}\}Br^a_6]$ was extracted using 3 ml of dichloromethane (the solid precipitate (KBr) was filtered). 7.7 mg of single crystals were obtained by slow diffusion of pentane; yield 19% taking into account **1** impurities. Single-crystal X-ray diffraction analysis revealed that **3** is strongly structurally correlated to the structure reported by Sokolov *et al.* and denoted 5c.³

*Preparation method of solutions of **1** for spectroscopic investigations.* They were prepared by dissolution of 20 mg of **1** per milliliter of solution. After stirring at 350 tr/min overnight, the solutions were filtered out to get rid of non-dissolved impurities. In the case of acetone, the dissolution was carried out in dried acetone under argon using Schlenk techniques. After 24 hours, stirring was stopped. After decantation, a green solution is obtained. The green solution turned instantaneously brown when opening the Schlenk tube. When solubilizing **1** in acetone in atmospheric condition using the same protocol, a brown solution is obtained since the early stage of dissolution. The solutions obtained from **1** after filtration in water and acetone will be denoted $\mathbf{1}_{water}$ and $\mathbf{1}_{acetone}$ respectively.

Raman solid-state measurements. Raman scattering spectra from 1100 cm^{-1} to 100 cm^{-1} were acquired for **1**, $\mathbf{2}_{\alpha,\beta,\gamma}$ and **3** compounds as powders at room temperature using a LabRamHigh resolution spectrometer coupled with a confocal microscope (Horiba Jobin Yvon), 600 g/mm gratings and $10 \times$ objective. A He-Ne 633 nm laser was used for scattering excitation. Raman spectra were recorded at room temperature with 100 s exposition and 2 accumulations. The calibration of the Raman spectrometer was performed using the main Raman band of silicon

wafer (520 cm^{-1}). A soda-lime glass sample holder was used in all cases except for **2 γ** . Indeed, the smaller quantity of **2 γ** synthesized prevent us to use the same sample holder. A silicon monocrystalline sample holder usually used for XRPD data collection was thus utilized. The signal-to-noise ratio obtained is importantly reduced compare to the other recordings.

UV-vis spectrometry. Absorption spectra of the solutions were measured by a high-performance UV-Vis-NIR spectrophotometer Perkin Elmer Cary 5000 in a range 200 nm – 2000 nm. Internal diffuse reflectance spectra measurements on sample powder were also measured by a UV-Vis-NIR spectrophotometer Varian Cary 5000 in a range 200 nm – 2000 nm by means of an integrating sphere. Solutions of $8.5 \times 10^{-8} \text{ mol.L}^{-1}$ in $\{\text{Ta}_6\text{Br}_{12}^{\text{I}}\}$ -containing species.

Mass Spectrometry. Mass spectrometry (ESI-MS) measurements with ionization by electrospray or nanospray source were recorded on a quadrupole time-of-flight mass spectrometer (microtof-Q, Bruker-Daltonics, Bremen, Germany). The samples **1**, **2 β** , and **3** were analyzed both in negative and positive ion mode. Each solution sample was prepared to approximately $50 \text{ }\mu\text{mol.L}^{-1}$ (residual impurities preventing to attain a completely quantitative concentration) in the following different solvents: water, dichloromethane, and acetone. The water solutions were infused directly in an electrospray source using a syringe pump (flow rate $180 \text{ }\mu\text{L.h}^{-1}$) and the ESI process was assisted with a dry gas at 80°C . The acetone and dichloromethane solutions were infused directly in a nanospray source with dry gas temperature set at 55°C .

Thermogravimetric analyses (TGA). TGA were performed in air on a Netzsch STA 449 F3 Jupiter thermobalance. The powder samples of 35 mg were loaded in an alumina crucible and heated in N_2 gas flow at a rate of $1 \text{ }^\circ\text{C.min}^{-1}$ up to $400 \text{ }^\circ\text{C}$.

Chemical analyses. Chemical analyses were evaluated on a FlashEA1112Series device from ThermoFinnigan. It is composed of a combustion tube, a chromatographic column and a TCD

detector. Samples were weight with high precision and placed on a tin crucible before being oxidized in a combustion furnace. The generate vapors are then sorted by chromatography. Carbon, hydrogen, nitrogen and suffer proportion are determined thanks to its dedicated calibration curve.

Powder X-Ray diffraction experiments. X-Ray powder diffraction (XRPD) data were collected at room temperature using a Bruker D8 Advance two-circle diffractometer (θ - 2θ Bragg-Brentano mode) using Cu K α radiation ($\lambda = 1.54056 \text{ \AA}$) equipped with a Ge(111) monochromator and a Lynx Eye detector. The analyses of the diffraction patterns were performed by profile refinement using the FullProf and WinPlotr software packages.⁴

Temperature dependent X-Ray powder diffraction experiments. XRPD versus temperature were recorded using a Rigaku SmartLab diffractometer using Cu K α_1 radiation ($\lambda = 1.54056 \text{ \AA}$) equipped with a diffracted beam monochromator (Johansson-type X-ray mirror) and a D/teX Ultra 250 detector. XRD profiles were recorded under N₂ atmosphere. The initial temperature was of 25°C and was increased up to 400°C by steps of 25°C, with 3°C/min as a heating rate. At each 25°C step, an X-ray powder pattern was recorded between 7° and 100° (2θ) with a scan speed of 4°/min and a step of 0.02 deg. The analyses of the diffraction patterns were performed by profile refinement using the FullProf and WinPlotr software packages.⁴

Electrochemical solution measurements. The electrochemical characterization by cyclic voltammetry was performed at room temperature using a conventional three-electrode cell in the Ta₆-containing electrolytic solution. This solution consists of 1 mM of **3** in a solution of 0.1 M of tetrabutylammonium hexafluorophosphate (TBA)[PF₆] in dichloromethane (column chromatography purification). A glassy carbon electrode was used as working electrode, a platinum wire as counter-electrode, and an Ag/AgCl electrode as reference electrode. The solution was degassed by N₂ before performing the electrochemical measurements. It has to be noticed that, even if limited, some solvent evaporation occurs during the measurements leading

to slight changes in the solution concentration. The cyclic voltammetry scans were recorded in a potential window of -0.45 V to 0.45 V versus Ag/AgCl at 0.1 V.s⁻¹ using a Metrohm Autolab PGSTAT30. Negative potentials were applied from the initial equilibrium potential (around 0.25 V vs Ag/AgCl) leading to anodic currents.

Determination of 2_α and 2_β number of water molecules based on temperature-dependent XRPD and TGA measurements. The determination of water content in 2_α and 2_β was done by combining temperature dependent and thermogravimetric analyses (TGA) (Fig. S5, S6, S7). For both 2_α and 2_β , a structural transition towards a same phase 2_δ is observed. A closer look to the temperature-dependent XRPD patterns shows that this phase transition is completed at different temperatures, starting at 175°C and 125°C for 2_α and 2_β respectively. The two main diffraction peaks of 2_δ are shifted to higher angles compared to the two main peaks of 2_α and 2_β . Such a shift indicates a contraction of the unit cell concomitant with the loss of water molecules. Above 275°C, the two main diffraction peaks of 2_δ disappear, indicating decomposition to amorphous phases. TGA experiments under N₂ for 2_α and 2_β are shown in Figure S5. In order to facilitate the comparison, the results of 2_α are corrected by removing the impurities from the global mass of the sample. The resulting plots reveal that the structural transitions $2_\alpha/2_\delta$ and $2_\beta/2_\delta$ are associated with a weight loss of roughly 6.9 % and 3.5 %, respectively, attributed to the loss of different amounts of water molecules.

In the following demonstration, we will consider the general formula $[\{\text{Ta}_6\text{Br}_{12}\}\text{Br}_2(\text{H}_2\text{O})_4]\cdot x\text{H}_2\text{O}$ for both systems. 2_α and 2_β contain $x_{2\alpha}$ and $x_{2\beta}$ crystallization water molecules, respectively. Contrarily to 2_β , 2_α samples contain KBr and water-soluble amorphous phases. These differences of initial sample compositions were taken into account in our calculations of $x_{2\alpha}$ and $x_{2\beta}$. The total weight loss for $[\{\text{Ta}_6\text{Br}_{12}\}\text{Br}_2(\text{H}_2\text{O})_4]\cdot x\text{H}_2\text{O}$ could correspond either to the loss of the x crystallization water molecules or to the loss of both the x crystallization water molecules and the 4 apical water molecules directly coordinated to the

cluster units. Considering the TGA of $\mathbf{2}_\beta$, values of $x_{2\beta}$ up to 8 were tested considering these two schemes of water loss. The best fit allows to conclude that the decrease of weight of 3.5 % corresponds to the loss of 4 H₂O crystallization molecules for the formula $[\{\text{Ta}_6\text{Br}_{12}\}\text{Br}_2(\text{H}_2\text{O})_4]\cdot 4\text{H}_2\text{O}$. Considering the TGA analyses of $\mathbf{2}_\alpha$, values of $x_{2\alpha}$ up to 12 were tested considering the two schemes of water loss. The best fit allows to conclude that the decrease of weight of 6.9 % occurs to the loss of 10 H₂O crystallization molecules for the formula $[\{\text{Ta}_6\text{Br}_{12}\}\text{Br}_2(\text{H}_2\text{O})_4]\cdot 10\text{H}_2\text{O}$. In those models, the loss of all the crystallization water molecules (10 for $\mathbf{2}_\alpha$ and 4 for $\mathbf{2}_\beta$) leads to the same $[\{\text{Ta}_6\text{Br}_{12}\}\text{Br}_2(\text{H}_2\text{O})_4]$ formula for the compound which is labelled $\mathbf{2}_\delta$. Considering that the evaporation of a different number of crystallization water molecules requests different amounts of energy, the different $\mathbf{2}_\alpha/\mathbf{2}_\delta$ and $\mathbf{2}_\beta/\mathbf{2}_\delta$ transition temperatures detected by high temperature XRPD analyses can be explained by a kinetic effect.

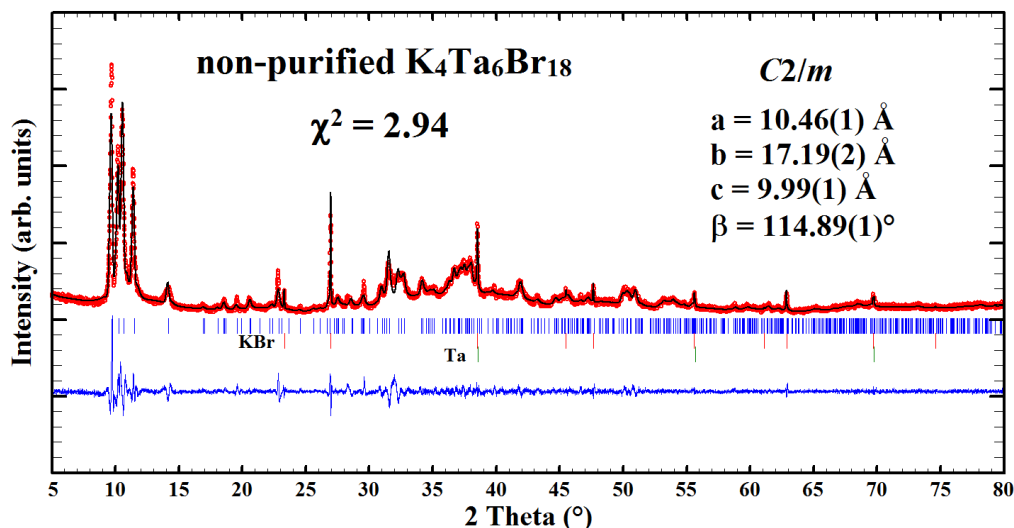


Figure S1. Le Bail refinement of the XRPD pattern of **1** recorded at room temperature.

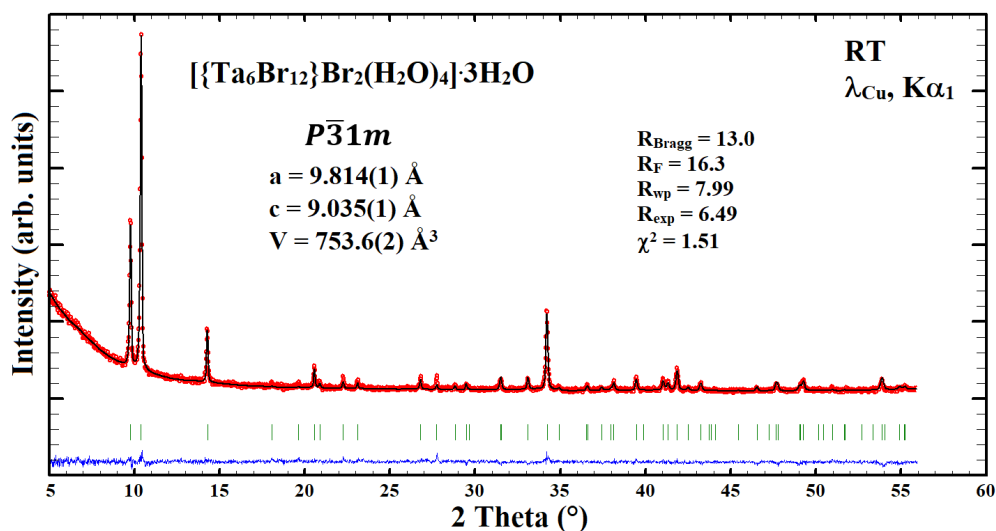


Figure S2. Rietveld refinement of the XRPD pattern of the 2_γ sample recorded at room temperature.

Table S1. Refined atomic coordinates of the 2_γ compound obtained from Rietveld refinement of the room temperature XRPD pattern.

Atom	Site	x	y	z	SOF
Ta1A	$6k$	0.222(3)	0	0.192(3)	0.33
Ta1B	$6k$	0.164(2)	0	0.103(2)	0.67
Br1A	$6k$	0.120(5)	0	0.812(5)	0.33
Br1B	$6k$	0.211(2)	0	0.662(3)	0.67
Br2	$6i$	0.211(1)	0.789(1)	0	1.00
Br3	$6k$	0.414(5)	0	0.314(5)	0.33
O1	$6k$	0.368(10)	0	0.417(12)	0.67
O2	$6j$	0.156(6)	0.844(6)	1/2	0.50

Table S2. Interatomic distances (Å) in the motif $[\{\text{Ta}_6\text{Br}_{12}\}\text{Br}_2(\text{H}_2\text{O})_4]$ deduced from Rietveld refinement of the room temperature XRD data of 2_γ .

Ta1A-Ta1B	3.392(30) ($\times 4$)
	3.307(33) ($\times 4$)
Ta1B-Ta1B	2.793(22) ($\times 2$)
	2.463(24) ($\times 2$)
$\overline{d_{\text{Ta-Ta}}}$	3.11
Ta1A-Br1B	2.501(3) ($\times 4$)
Ta1A-Br2	2.664(9) ($\times 4$)
Ta1B-Br1A	1.636(13) ($\times 4$)
Ta1B-Br1B	2.837(10) ($\times 4$)
Ta1B-Br2	2.516(7) ($\times 8$)
$\overline{d_{\text{Ta-Br}^t}}$	2.45
Ta1A-Br3	2.18(8)
Ta1A-O1	2.49(17)
Ta1B-Br3	3.11(7)
Ta1B-O1	3.47(16)
$\overline{d_{\text{Ta-O}^a}}$	3.00

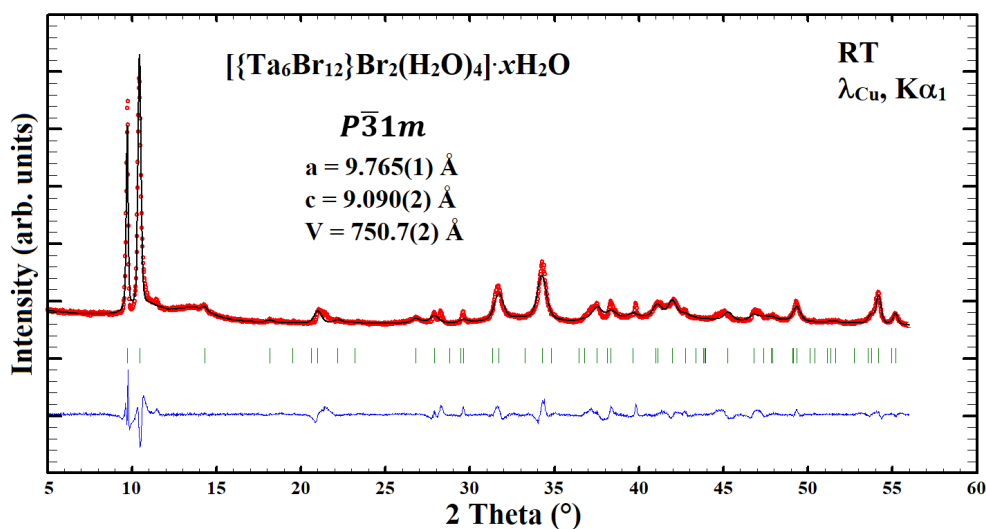


Figure S3. Le Bail refinement of the room temperature XRPD pattern of the large batch of 2_β powder.

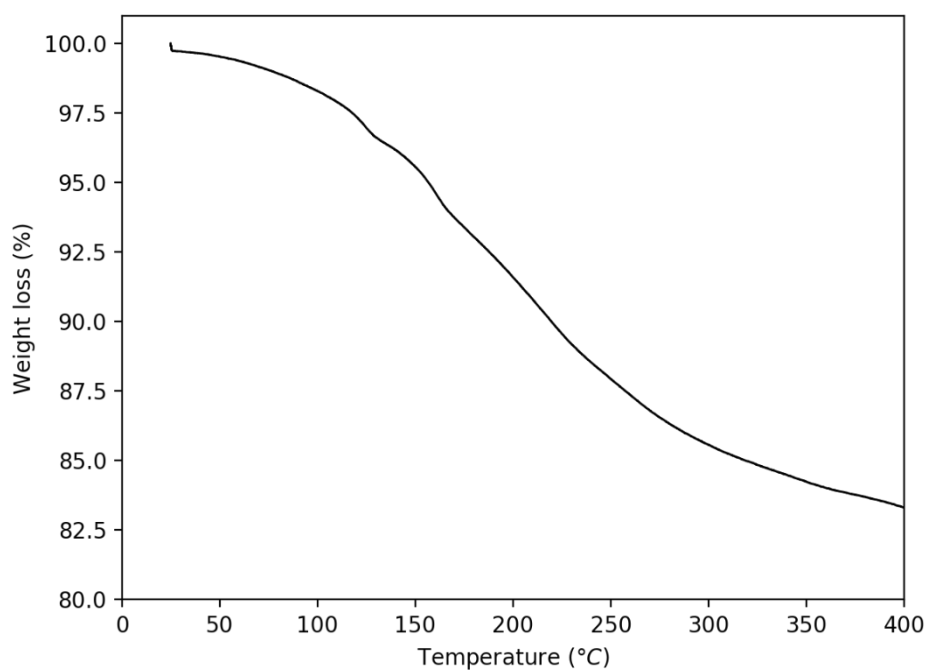
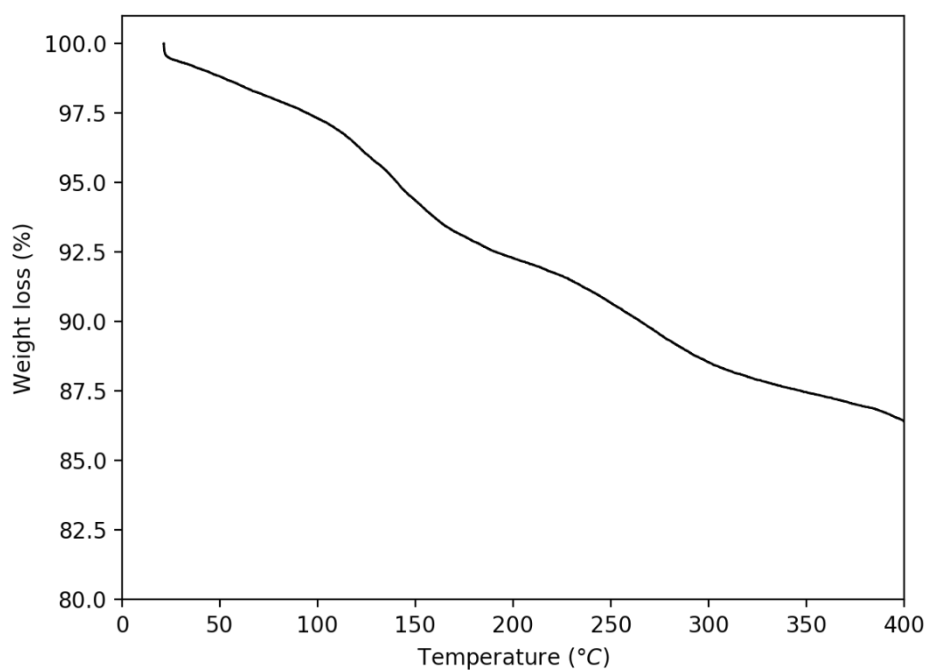
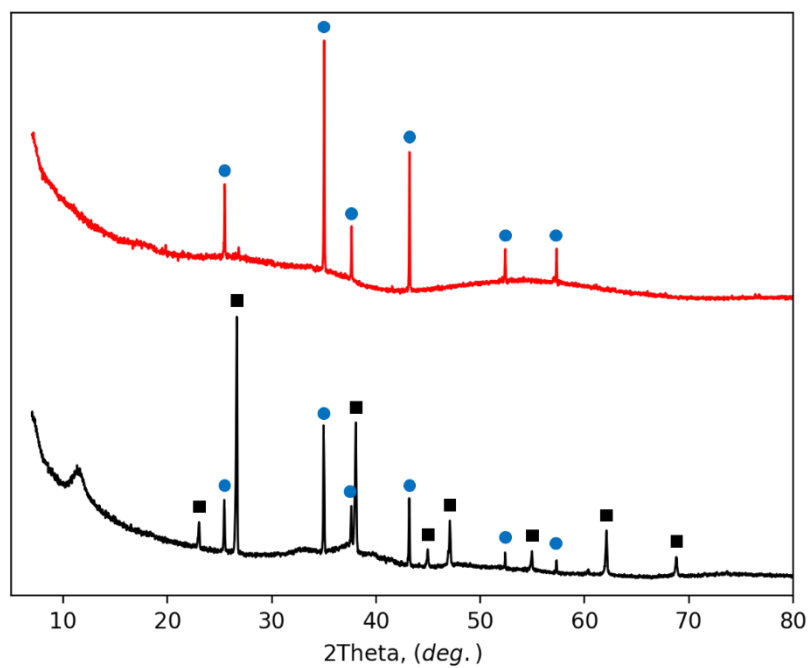
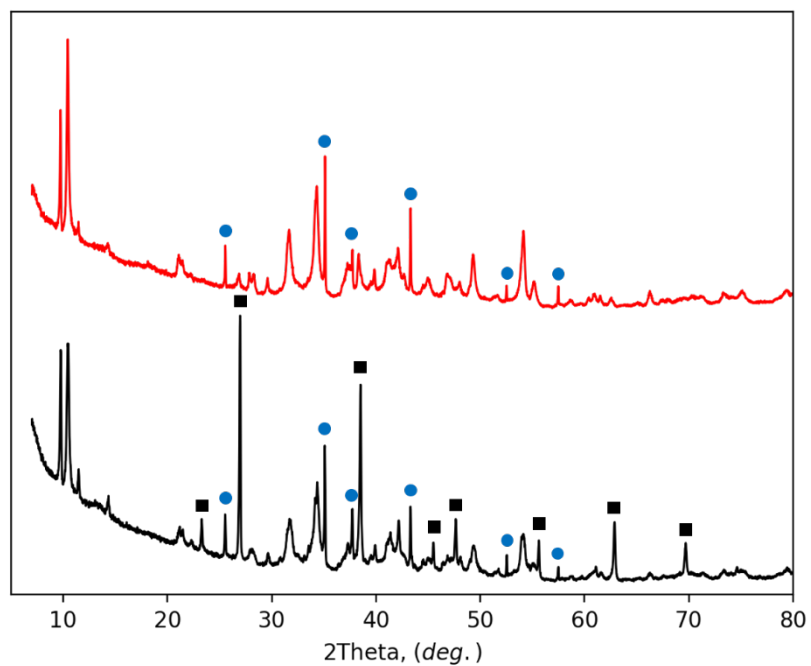


Figure S4. Thermal gravimetric analysis (TGA) of **2_α** (top) and **2_β** (bottom). For sake of comparison between the two systems, the TGA results **2_α** were corrected to take into account the presence of impurities in the sample: $[\text{Weight loss (T)}] = [\text{Measured weight loss(T)}] + 1324 \cdot [\text{Measured weight loss(T)}] / M(\mathbf{2}_\alpha)$



Figure

Figure S5. Top: XRPD pattern recorded at 25°C on alumina holders of powders of 2_α in black and 2_β in red. Bottom: XRPD pattern recorded at 400°C on alumina holders of 2_α in black and 2_β in red (following the temperature increase procedure described in the main text). Blue dots: Al_2O_3 . Black square: KBr.

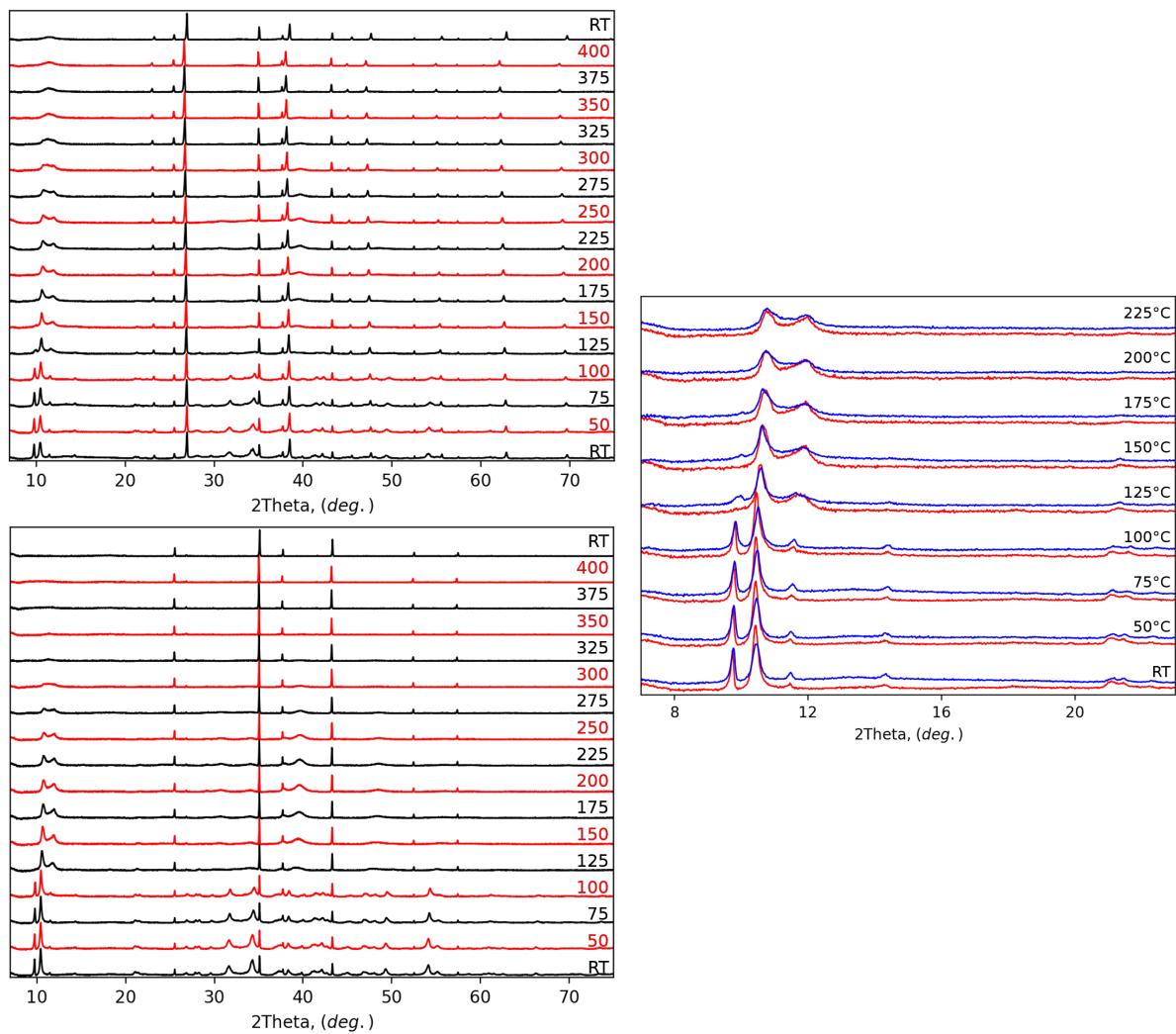


Figure S6. XRPD patterns recorded under N_2 atmosphere from 25°C to 400°C on alumina holders of 2α (top left) and 2β (bottom left). Comparison of XRPD patterns in the 2θ domain 7 - 23° of 2α (blue) and 2β (red) recorded at temperatures ranging from 25°C to 225°C (right).

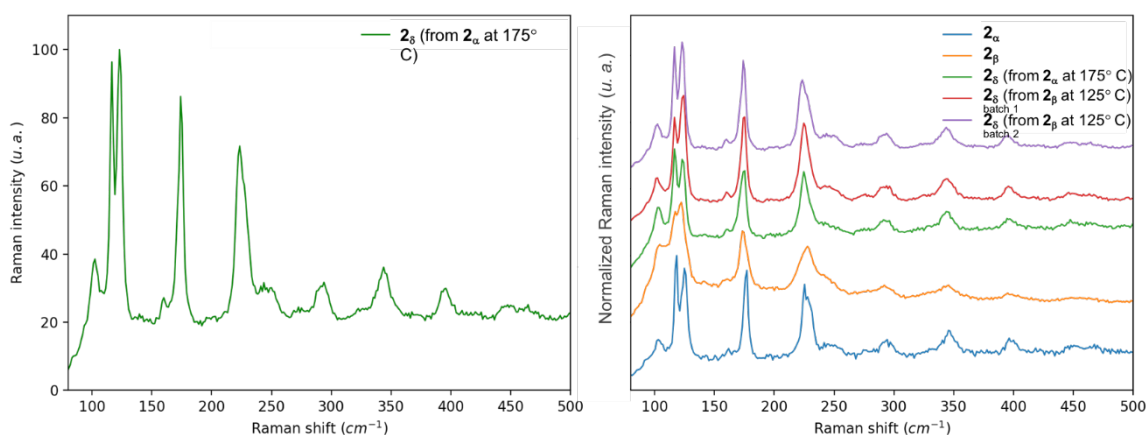


Figure S7. Left: normalized Raman spectra of 2_δ obtained by heating of 2_α at 175°C . Right: comparison between of 2_α , 2_β and 2_δ obtained by heating i) 2_α at 175°C and ii) two different batches of 2_β at 125°C .

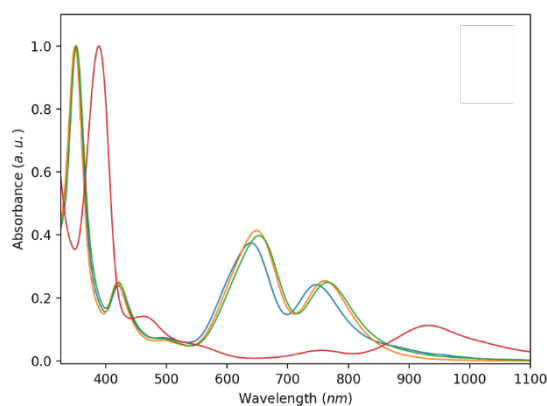


Figure S8. Normalized UV-visible absorption spectra of solution **1** at RT in water (blue spectrum), methanol (orange spectrum), ethanol (green spectrum), acetone (red spectrum).

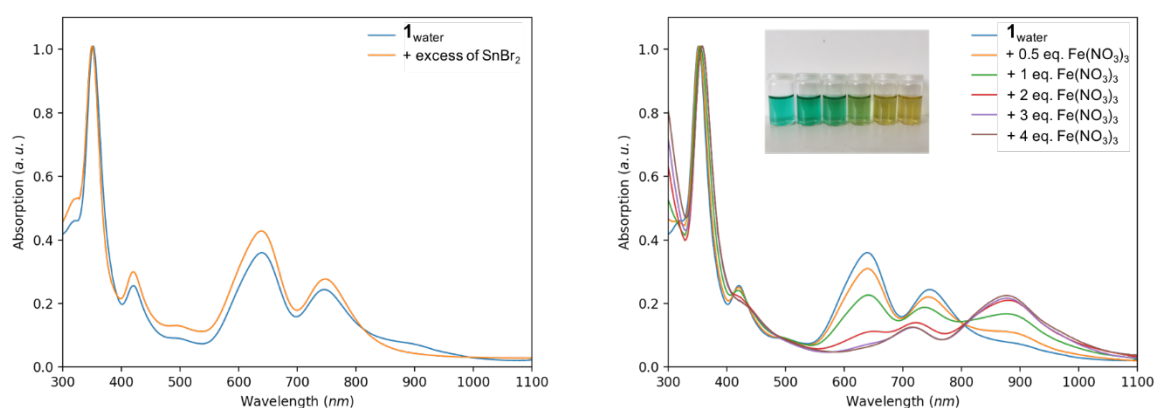


Figure S9. Normalized UV-visible absorption spectra of solution **1** at RT in water (blue spectrum). Left: addition of SnBr_2 in excess. Right: addition of 0.5 to 4 equivalent of $\text{Fe}(\text{NO}_3)_3$.

Computational details.

Molecular density functional (DFT) calculations were carried out using the Amsterdam Density Functional (ADF 2019) suite of programs developed by Baerends and co-workers.⁵ The revPBE exchange and correlation nonlocal gradient corrections⁶ were added to the local density approximation description.⁷ Relativistic effects were treated at the first-order of perturbation theory using a ZORA Hamiltonian.⁸ The all-electron ADF QZ4P Slater-type atomic basis set was used, *i.e.* a quadruple- ζ STO basis set completed with four polarization functions. This procedure was successfully employed to study the ground state and optical properties of $[\{\text{Mo}_6\text{Br}_8^i\}\text{Br}_6^a]^{2-}$ and $[\{\text{Mo}_6\text{Br}_8^i\}(\text{NCS})_6^a]^{2-}$ metal cluster in good agreement with experimental results.⁹ Geometry optimizations of the cluster units were performed without symmetry constraint. If the final geometries were presenting symmetry elements (variation of distances $< 0.001 \text{ \AA}$), the symmetry was later imposed (validation by checking of total energy). For the oxidized compounds (valence electron concentration (VEC) = 14), the triplet spin state configurations were calculated. They are less stable in energy in all cases and thus they were not investigated further. Vibrational frequency calculations were performed to check the local minimum character of all systems. Raman (laser frequency 1.958 eV / 633 nm), IR, and UV-visible spectroscopic properties were simulated using the modules provided in ADF Modeling suite. Dispersion correction developed by Grimme and collaborators was added to the total bonding energy and gradients when “Grimme” is stipulated in the text.¹⁰ Conductor-like screening model of solvation (COSMO, water or acetone solvent effect) was used when specified for geometry optimizations and TD-DFT calculations.¹¹ The Cartesian coordinates of all optimized structures are given in Table S3.

Table S3. Cartesian coordinates of the optimized geometries [$\{\text{Ta}_6\text{Br}_{12}^i\}\text{Br}_6^a\}^{4-}$ ($n = 2-4$) (O_h symmetry), [$\{\text{Ta}_6\text{Br}_{12}^i\}(\text{H}_2\text{O})_4^a\}^{2+}$], [$\{\text{Ta}_6\text{Br}_{12}^i\}(\text{OH})_6^a\}^{4-}$], [$\{\text{Ta}_6\text{Br}_{12}^i\}(\text{H}_2\text{O})_6^a\}^{2+}$], [$\{\text{Ta}_6\text{Br}_{12}^i\}trans\text{-}(\text{OH})_2(\text{OH}_2)_4^a\}$], [$\{\text{Ta}_6\text{Br}_{12}^i\}trans\text{-Br}_2(\text{H}_2\text{O})_4^a\}$], [$\{\text{Ta}_6\text{Br}_{12}^i\}trans\text{-Br}_2(\text{H}_2\text{O})_4^a\}.4\text{H}_2\text{O}$ (*Grimme*)

$\{\text{Ta}_6\text{Br}_{12}^i\}\text{Br}_6^a\}^{4-}$			Br	0.000000	0.000000	-4.934172	
Ta	0.000000	-2.094874	0.000000	Br	2.578595	-2.578595	0.000000
Ta	-2.094874	0.000000	0.000000	Br	-2.578595	2.578595	0.000000
Ta	0.000000	2.094874	0.000000	Br	-2.578595	-2.578595	0.000000
Ta	0.000000	0.000000	2.094874	Br	0.000000	2.578595	-2.578595
Ta	2.094874	0.000000	0.000000	Br	-4.934172	0.000000	0.000000
Ta	0.000000	0.000000	-2.094874	Br	-2.578595	0.000000	-2.578595
Br	-2.597091	0.000000	2.597091	Br	0.000000	-2.578595	2.578595
Br	2.597091	2.597091	0.000000	Br	-4.934172	0.000000	0.000000
Br	0.000000	-2.597091	2.597091	Br	0.000000	-4.934172	0.000000
Br	2.597091	0.000000	2.597091	$\{\text{Ta}_6\text{Br}_{12}^i\}(\text{H}_2\text{O})_4^a\}^{2+}$			
Br	2.597091	0.000000	-2.597091	Ta	-0.054398	-1.957554	0.166744
Br	0.000000	2.597091	2.597091	Ta	0.039736	0.068474	2.179264
Br	0.000000	5.080565	0.000000	Ta	-2.091675	0.046325	0.152964
Br	0.000000	0.000000	5.080565	Ta	-0.066335	-0.067177	-1.976182
Br	0.000000	0.000000	-5.080565	Ta	0.027943	1.958771	0.036308
Br	-2.597091	-2.597091	0.000000	Ta	2.065091	-0.045241	0.050131
Br	2.597091	2.597091	0.000000	Br	-0.000406	-2.540746	2.732371
Br	-2.597091	-2.597091	0.000000	Br	0.110180	2.707707	2.557710
Br	0.000000	2.597091	-2.597091	Br	-2.612834	-2.567761	0.254983
Br	5.080565	0.000000	0.000000	Br	2.475624	-2.679170	0.122638
Br	-2.597091	0.000000	-2.597091	Br	-2.530584	0.141431	2.751143
Br	0.000000	-2.597091	-2.597091	Br	-2.665740	-0.026718	-2.416811
Br	-5.080565	0.000000	0.000000	Br	2.503991	-0.139885	-2.548198
Br	0.000000	-5.080565	0.000000	Br	-2.502307	2.680504	0.080312
$\{\text{Ta}_6\text{Br}_{12}^i\}\text{Br}_6^a\}^{3-}$			Br	-0.025929	2.542209	-2.529301	
Ta	0.000000	2.133188	0.000000	Br	-0.136390	-2.706206	-2.354682
Ta	0.000000	0.000000	-2.133188	Br	2.586707	2.568975	-0.051963
Ta	0.000000	0.000000	2.133188	Br	2.638995	0.028428	2.620143
Ta	2.133188	0.000000	0.000000	H	-0.165520	-0.613635	5.072733
Ta	0.000000	-2.133188	0.000000	H	-4.947028	0.869109	-0.087938
Ta	-2.133188	0.000000	0.000000	H	4.920000	-0.860739	0.314512
Ta	2.587910	0.000000	2.587910	H	0.129316	0.616787	-4.870056
Br	2.587910	0.000000	-2.587910	O	0.154615	0.145287	4.555852
Br	0.000000	0.000000	4.985836	H	-0.152454	0.940626	5.023535
Br	-2.587910	2.587910	0.000000	O	4.441561	-0.103842	-0.064657
Br	2.587910	2.587910	0.000000	H	4.949977	0.688292	0.179730
Br	0.000000	4.985836	0.000000	H	-4.976812	-0.683324	-0.001459
Br	0.000000	-2.587910	-2.587910	O	-0.182189	-0.145212	-4.352384
Br	-2.587910	0.000000	2.587910	H	0.131360	-0.937569	-4.820819
Br	0.000000	2.587910	2.587910	O	-4.468834	0.100866	0.268062
Br	0.000000	2.587910	-2.587910	$\{\text{Ta}_6\text{Br}_{12}^i\}(\text{OH})_6^a\}^{4-}$			
Br	0.000000	-2.587910	2.587910	Ta	-0.007826	0.017273	2.131541
Br	2.587910	-2.587910	0.000000	Ta	-2.131380	-0.011281	-0.019040
Br	4.985836	0.000000	0.000000	Ta	0.022467	-2.131411	0.005854
Br	0.000000	-4.985836	0.000000	Ta	2.131425	0.011138	0.019158
Br	-2.587910	0.000000	-2.587910	Ta	-0.022560	2.131447	-0.005969
Br	0.000000	0.000000	-4.985836	Ta	0.007943	-0.017187	-2.131398
Br	-4.985836	0.000000	0.000000	Br	-0.000295	-2.645854	2.735962
Br	-2.587910	-2.587910	0.000000	Br	-0.012704	2.658356	2.658851
$\{\text{Ta}_6\text{Br}_{12}^i\}\text{Br}_6^a\}^{2-}$			Br	-2.639163	-2.742744	0.001645	
Ta	0.000000	-2.169160	0.000000	Br	-2.738447	-0.010976	2.643642
Ta	-2.169160	0.000000	0.000000	Br	2.639115	2.742636	-0.001954
Ta	0.000000	2.169160	0.000000	Br	2.738619	0.010804	-2.643451
Ta	0.000000	0.000000	2.169160	Br	-0.000093	2.646043	-2.736145
Ta	2.169160	0.000000	0.000000	Br	-2.664760	2.652421	-0.005689
Ta	0.000000	0.000000	-2.169160	Br	-2.656596	-0.010485	-2.660359
Br	2.578595	0.000000	2.578595	Br	0.012886	-2.658073	-2.659129
Br	2.578595	2.578595	0.000000	Br	2.664669	-2.652492	0.006257
Br	0.000000	-2.578595	2.578595	Br	2.656722	0.010157	2.660576
Br	2.578595	0.000000	2.578595	O	-0.046447	0.108729	4.246108
Br	2.578595	0.000000	2.578595	H	0.005653	-0.808752	4.555539
Br	0.000000	2.578595	2.578595	O	4.245767	0.052783	0.112622
Br	0.000000	4.934172	0.000000	H	4.556141	0.004132	-0.804725
Br	0.000000	0.000000	4.934172	O	0.119064	-4.245764	0.042117
				H	-0.797773	-4.557317	-0.008511

O	0.046414	-0.108311	-4.245907	Br	0.17443222	2.64744479	2.64597790
H	-0.005132	0.809253	-4.555162	Br	-2.68595695	-2.51063251	0.32464715
O	-4.245722	-0.053089	-0.112468	Br	2.56849694	-2.61353330	0.04411002
H	-4.555915	-0.004589	0.804955	Br	-2.47360343	0.13449256	2.84115126
O	-0.119442	4.245744	-0.042727	Ta	-2.04131721	0.04192293	0.21369634
H	0.797371	4.557404	0.007807	Ta	-0.12709619	-0.06082474	-1.92574532
$[\{Ta_6Br_{12}\}(OH)_6]^{2-}$							
Ta	0.094955	-2.180399	0.211295	Br	-2.75579391	-0.02834304	-2.35943448
Ta	-0.379249	0.163968	2.117666	Br	2.44641504	-0.13186136	-2.63848513
Br	0.282919	-2.394085	2.840800	Br	-2.59464360	2.61700307	0.15897790
Br	-0.642712	2.818004	2.325144	H	-0.25858050	-0.60159770	4.94016483
Br	-2.454992	-2.836717	-0.150018	H	-4.81447882	0.84972490	-0.14199314
Br	2.717949	-2.402937	0.588729	H	4.78605519	-0.85961119	0.31366063
H	0.388861	-4.709530	-0.304383	Ta	0.02452553	2.14026060	0.03254717
Br	-3.075714	-0.049393	2.169659	Br	-0.10932834	2.48385165	-2.60564475
Ta	-2.231018	-0.201077	-0.337983	Br	-0.20134819	-2.64412518	-2.44338695
Ta	0.277245	-0.192694	-2.109766	Br	2.65820988	2.51413575	-0.12169116
Br	-2.235276	-0.413226	-2.960733	H	0.24639107	0.59983663	-4.73567288
Br	2.973754	0.020723	-2.161749	Br	2.72858887	0.03125405	2.56236655
Br	-2.819914	2.374253	-0.580772	Ta	2.01422457	-0.03788435	-0.01084230
H	-4.788834	-0.380160	0.055334	O	0.26149670	0.13679208	4.57794157
Ta	-0.196906	2.151687	-0.203427	H	-0.18306101	0.94536247	4.88726866
Br	0.181009	2.365358	-2.832920	O	4.46311830	-0.08031479	-0.17169183
Br	0.540738	-2.846699	-2.317276	H	4.81333585	0.68996008	0.30888800
Br	2.353021	2.808001	0.157944	Br	0.07263875	4.82720489	-0.05314323
Br	2.133283	0.384560	2.968648	O	-0.28744806	-0.12911395	-4.37440581
Ta	2.129048	0.172370	0.345895	H	0.14313210	-0.94551955	-4.68318487
O -	0.735562	0.446274	4.143074	O	-4.49088681	0.09049710	0.37360251
H -	0.584495	-0.362733	4.653863	H	-4.84040728	-0.69840320	-0.07641058
O	4.151591	0.349472	0.760069	Br	-0.09925333	-4.82313501	0.25613416
H	4.686863	0.351488	-0.047413	$[\{Ta_6Br_{12}\}trans-Br_2(H_2O)_4].4H_2O$ Grimme			
O -	0.322813	4.199714	-0.511423	Ta	-0.008606	-2.142842	0.025656
H -	0.490966	4.680802	0.312206	Ta	0.230854	-0.072407	2.052081
O	0.633544	-0.475051	-4.135172	Br	0.213920	-2.640996	2.607556
H	0.483348	0.334176	-4.645868	Br	0.342176	2.485448	2.619117
O	-4.253564	-0.378182	-0.752148	Br	-2.603323	-2.568235	0.251080
O	0.220875	-4.228429	0.519274	Br	2.564953	-2.666345	-0.241139
$[\{Ta_6Br_{12}\}(OH)_6]^{2-}$							
Ta	-0.054894	-1.957450	0.167222	Br	-2.281408	-0.026964	2.855399
Ta	0.039490	0.069295	2.179465	Ta	-1.993885	-0.022782	0.232860
Br	-0.000706	-2.540395	2.733599	Ta	-0.174861	-0.049189	-1.991900
Br	0.110061	2.708769	2.557797	Br	-2.795684	-0.000908	-2.280940
Br	-2.613707	-2.567877	0.255564	Br	2.337640	-0.096970	-2.794317
Br	2.475448	-2.679706	0.123063	Br	-2.516045	2.547660	0.307078
Br	-2.531257	0.141418	2.751515	H	0.094899	-0.863093	4.817999
Ta	-2.092079	0.046718	0.152977	H	-4.758915	0.789733	0.087830
Ta	-0.066573	-0.067124	-1.976041	H	4.811525	-0.912815	-0.029817
Br	-2.666078	-0.026551	-2.417305	Ta	0.056315	2.025045	0.034593
Br	2.503977	-0.139856	-2.548341	Br	-0.159277	2.517609	-2.549057
Br	-2.502899	2.681192	0.080620	Br	-0.282265	-2.606317	-2.560350
H	-0.138288	-0.616182	5.074262	Br	2.651883	2.456381	-0.204606
H	-4.947196	0.867609	-0.095840	H	-0.030870	0.739887	-4.758021
H	4.918644	-0.865329	0.304543	Br	2.850773	-0.117939	2.340306
Ta	0.027694	1.959303	0.036339	Ta	2.047898	-0.096224	-0.172759
Br	-0.026367	2.542743	-2.529641	O	0.510186	-0.086545	4.403773
Br	-0.136992	-2.706620	-2.354544	H	0.097217	0.680701	4.836180
Br	2.586802	2.569388	-0.051868	O	4.399615	-0.138068	-0.450289
H	0.130801	0.617535	-4.869020	H	4.832577	0.630622	-0.040111
Br	2.639285	0.029058	2.620289	H	-4.777504	-0.753989	0.107266
Ta	2.064795	-0.045158	0.050229	O	-0.450328	-0.034313	-4.343863
O	0.155967	0.151894	4.555414	H	-0.034878	-0.803712	-4.770341
H	-0.175206	0.937656	5.022866	O	-4.345632	0.018009	0.512533
O	4.441155	-0.103426	-0.065721	Br	0.110522	4.835230	0.028492
H	4.949537	0.685235	0.189747	Br	-0.068650	-4.958212	0.045317
H	-4.976958	-0.684070	0.003516	O	3.115676	6.405802	-0.577190
O	-0.181751	-0.144564	-4.352145	H	3.343426	6.469177	-1.519082
H	0.132032	-0.936875	-4.820501	H	2.326579	5.822660	-0.570734
O	-4.469073	0.102379	0.266628	H	-1.719911	5.087164	-1.643800
$[\{Ta_6Br_{12}\}trans-Br_2(H_2O)_4]$							
Ta	-0.05146202	-2.13619752	0.17041237	O	-2.426826	5.322715	-2.280348
Ta	0.10005900	0.06458975	2.12874986	H	-2.467181	6.290730	-2.216867
Br	0.08259064	-2.48015890	2.80911155	H	-2.956196	-6.587002	1.885748
				O	-3.035109	-5.636358	1.702777
				H	-2.202672	-5.429680	1.226759
				O	2.644902	-5.428914	2.201397
				H	1.845540	-5.235751	1.671759
				H	2.715592	-6.395884	2.143649

$[\{Ta_6Br_{12}^i\}(OH)_5(OH)_1]^{1+}$			H	0.500684	0.677831	4.859423
Ta	0.147395	-2.124065	0.284080	H	-4.644279	1.323562
Ta	0.054248	0.214830	2.106958	H	4.657345	-1.361213
Br	0.222021	-2.257558	2.982105	Ta	0.216648	2.134148
Br	-0.100970	2.859112	2.390533	Br	0.210529	2.665745
Br	-2.455033	-2.722882	0.405914	Br	-0.297779	-2.459674
Br	2.820936	-2.378047	0.244103	Br	2.8982	2.289991
H	-0.346513	-4.711963	0.566113	H	-0.218437	-0.723164
H	0.208987	4.943152	0.279289	Br	2.6467	-0.329506
Br	-2.524616	0.123112	2.731525	Ta	2.031269	-0.200066
Ta	-2.026779	-0.129724	0.131101	O	0.033732	-0.124183
Ta	-0.039104	-0.198192	-1.966010	H	0.593681	-0.869873
Br	-2.643922	-0.402092	-2.441332	O	4.489389	-0.420951
Br	2.540507	-0.085382	-2.597132	H	4.812006	0.062561
Br	-2.755432	2.413713	-0.107779	O	0.390705	4.13726
H	0.833813	1.043831	4.825492	H	0.542041	4.670813
H	-4.871922	0.547913	0.474652	O	-0.035095	0.192732
H	4.883796	-0.527019	0.152679	H	-0.827554	0.69689
Ta	-0.128324	2.033600	-0.129736	O	-4.477302	0.362908
Br	-0.227480	2.342382	-2.766515	H	-4.761254	0.096068
Br	0.097757	-2.797306	-2.333342	O	-0.258129	-4.149703
Br	2.429411	2.742771	-0.268832			
H	-0.014084	-1.286211	-4.677651			
Br	2.661920	0.441400	2.578779			
Ta	2.044700	0.122853	0.009797			
O	0.056325	0.545764	4.517717			
H	0.097683	-0.309019	4.983432			
O	4.468708	0.338114	-0.017310			
H	4.803417	0.613648	-0.888862			
O	-0.347418	4.445031	-0.344063			
H	-0.115727	4.778436	-1.228305			
O	-0.048548	-0.354186	-4.395449			
H	-0.864960	0.002230	-4.787524			
O	-4.453177	-0.266672	0.145824			
H	-4.795716	-0.983442	0.707598			
O	0.394440	-4.096010	0.478853			
$[\{Ta_6Br_{12}^i\}trans-(OH)_2(OH)_4]^0$						
Ta	-0.190684	-2.133522	0.007868			
Ta	0.035662	-0.05567	2.100356			
Br	-0.205944	-2.626805	2.658293			
Br	0.296251	2.477797	2.80977			
Br	-2.848731	-2.333013	0.046101			
Br	2.419678	-2.818369	-0.064155			
H	-1.107147	-4.596154	0.052158			
Br	-2.564467	0.168533	2.721903			
Ta	-2.013589	0.182606	0.101885			
Ta	-0.023645	0.075022	-1.957051			
Br	-2.641647	0.333394	-2.497186			
Br	2.561211	-0.169735	-2.597803			
Br	-2.422651	2.802999	0.186323			

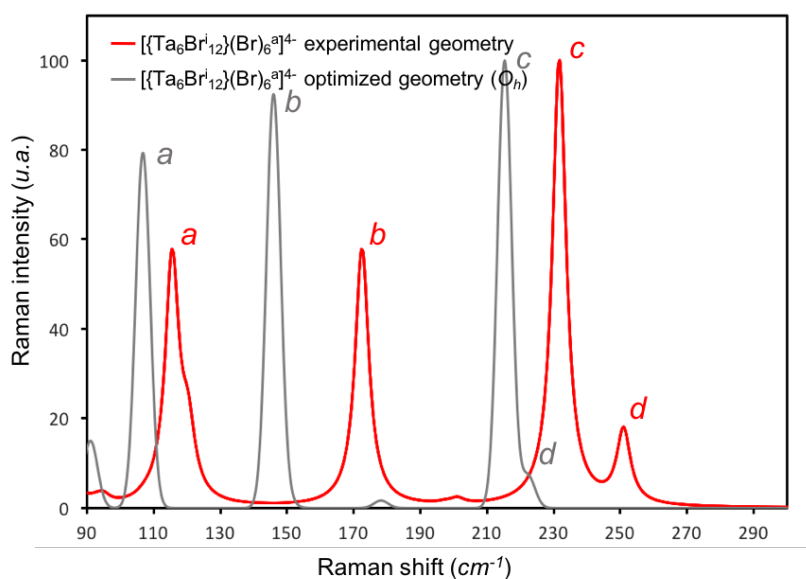
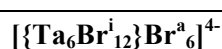


Figure S10. Simulated Raman spectra obtained using the geometry issued from the X-ray structure and the optimized geometries of $[\{Ta_6Br_{12}\}Br_6]^{4-}$ (O_h symmetry).

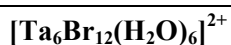
Table S4. Main TD-DFT vertical electronic singlet-singlet excitation energies (eV) oscillator strength (f), wavelength (nm), and composition for $[\{Ta_6Br_{12}\}Br_6]^{n-}$ ($n = 2-4$), $[\{Ta_6Br_{12}\}(H_2O)_6]^{2+}$, $[\{Ta_6Br_{12}\}(H_2O)_5(OH)^a]^+$, and $[\{Ta_6Br_{12}\}(H_2O)_4(OH)^a_4]$ in different geometries.

$[\{Ta_6Br_{12}\}Br_6]^{2-}$				
Electronic excitation energy (eV)	λ (nm)	f	Composition	
1.006	1231	0.008	HOMO-5 \rightarrow LUMO	87%
2.703	459	0.138	HOMO-1 \rightarrow LUMO+3	49%
			HOMO-2 \rightarrow LUMO+3	7%
4.049	306	0.075	HOMO-2 \rightarrow LUMO+6	20%
			HOMO-9 \rightarrow LUMO+2	18%
			HOMO-4 \rightarrow LUMO+4	17%
			HOMO-9 \rightarrow LUMO+3	6%
4.124	301	0.048	HOMO-9 \rightarrow LUMO+3	22%
			HOMO-9 \rightarrow LUMO+2	13%
			HOMO-4 \rightarrow LUMO+4	8%
4.565	272	0.279	HOMO-1 \rightarrow LUMO+11	46%
			HOMO \rightarrow LUMO+12	14%
			HOMO-11 \rightarrow LUMO+1	15%
$[\{Ta_6Br_{12}\}Br_6]^{3-}$				
Electronic excitation energy (eV)	λ (nm)	f	Composition	
1.476	839	0.012	HOSO α \rightarrow LUSO α	82%
			HOSO β -1 \rightarrow LUSO β	8%
2.794	444	0.023	HOSO α -13 \rightarrow LUSO α	35%
			HOSO α -4 \rightarrow LUSO α +3	15%
			HOSO α -7 \rightarrow LUSO α +3	10%
			HOSO β -1 \rightarrow LUSO β +4	10%

2.800	442	0.014	HOSO α -7 \rightarrow LUSO α +3	32%
			HOSO β -1 \rightarrow LUSO β +4	23%
			HOSO α -10 \rightarrow LUSO α	18%
			HOSO α -4 \rightarrow LUSO α +5	9%
3.996	310	0.018	HOSO β -10 \rightarrow LUSO β +9	26%
			HOSO α -25 \rightarrow LUSO α +3	23%
			HOSO α -13 \rightarrow LUSO α +9	16%
4.020	308	0.010	HOSO β -1 \rightarrow LUSO β +15	40%
			HOSO β -10 \rightarrow LUSO β +11	10%
			HOSO β -22 \rightarrow LUSO β +4	15%
			HOSO α -25 \rightarrow LUSO α +5	11%
4.069	305	0.021	HOSO α -4 \rightarrow LUSO α +14	45%
			HOSO α -25 \rightarrow LUSO α +1	13%
			HOSO α -1 \rightarrow LUSO α +22	8%



Electronic excitation energy (eV)	λ_{max} (nm)	f	Composition	
1.856	668	0.075	HOMO \rightarrow LUMO	74%
			HOMO \rightarrow LUMO+1	8%
			HOMO \rightarrow LUMO+2	8%
2.796	443	0.019	HOMO-1 \rightarrow LUMO+7	32%
			HOMO-1 \rightarrow LUMO+6	28%
			HOMO-4 \rightarrow LUMO+3	23%
3.002	413	0.004	HOMO-11 \rightarrow LUMO+2	21%
			HOMO-10 \rightarrow LUMO+2	16%
			HOMO-11 \rightarrow LUMO+1	13%
			HOMO-3 \rightarrow LUMO+7	9%
			HOMO-10 \rightarrow LUMO+1	8%
3.652	340	0.032	HOMO-4 \rightarrow LUMO+11	39%
			HOMO-6 \rightarrow LUMO+12	32%
			HOMO-6 \rightarrow LUMO+11	12%



Electronic excitation energy (eV)	λ (nm)	f	Nature	
1.982	626	0.024	HOMO \rightarrow LUMO+3	69%
			HOMO \rightarrow LUMO+4	69%
1.992	623	0.024	HOMO \rightarrow LUMO+4	63%
			HOMO \rightarrow LUMO+3	19%
			HOMO \rightarrow LUMO+5	9%
2.003	619	0.024	HOMO \rightarrow LUMO+5	82%
			HOMO \rightarrow LUMO+4	6%
3.476	357	0.011	HOMO-4 \rightarrow LUMO+7	34%
			HOMO-5 \rightarrow LUMO+6	13%
			HOMO-1 \rightarrow LUMO+9	6%

				HOMO-4→LUMO+2	6%
				HOMO-2→LUMO+8	5%
3.481	356	0.011		HOMO-6→LUMO+6	38%
				HOMO-3→LUMO+8	10%
				HOMO-6→LUMO+7	8%
				HOMO-4→LUMO+7	6%
3.485	356	0.010		HOMO-5→LUMO+7	30%
				HOMO-2→LUMO+9	9%
				HOMO-6→LUMO+6	8%
				HOMO-4→LUMO+7	6%
				HOMO-5→LUMO+2	5%
				HOMO-2→LUMO+13	48%
				HOMO-3→LUMO+13	21%
3.839	323	0.010		HOMO-1→LUMO+13	63%
3.843	323	0.011		HOMO-12→LUMO+5	12%
				HOMO-13→LUMO+5	11%
				HOMO-12→LUMO+3	11%
4.373	284	0.045		HOMO-13→LUMO+3	7%
				HOMO-13→LUMO+14	7%
				HOMO-8→LUMO+7	6%
				HOMO-13→LUMO+4	6%
				HOMO-12→LUMO+4	15%
				HOMO-14→LUMO+3	10%
				HOMO-14→LUMO+5	9%
4.376	283	0.042		HOMO-3→LUMO+14	9%
				HOMO-12→LUMO+3	6%
				HOMO-14→LUMO+4	6%
				HOMO-2→LUMO+14	5%
				HOMO-14→LUMO+5	17%
				HOMO-14→LUMO+3	13%
				HOMO-13→LUMO+3	12%
4.384	283	0.049		HOMO-2→LUMO+15	8%
				HOMO-1→LUMO+15	7%
				HOMO-13→LUMO+3	6%
				HOMO-9→LUMO+6	6%

[Ta₆Br₁₂(H₂O)₅(OH)]⁺				
Electronic excitation energy (eV)	λ (nm)	<i>f</i>	Nature	
1.880	659	0.018	HOMO→LUMO	87%
1.951	635	0.014	HOMO→LUMO+4	72%
			HOMO-1→LUMO	8%
			HOMO-1→LUMO+3	7%
2.000	619	0.017	HOMO→LUMO+5	73%
			HOMO-2→LUMO	11%
2.145	578	0.011	HOMO-1→LUMO+1	73%

			HOMO-2→LUMO+2	8%
			HOMO-2→LUMO+1	6%
2.936	422	0.016	HOMO-5→LUMO+5	35%
			HOMO-1→LUMO+7	29%
			HOMO-3→LUMO+7	7%
			HOMO-5→LUMO+6	6%
3.322	373	0.017	HOMO-2→LUMO+10	64%
			HOMO-6→LUMO+6	8%
			HOMO-4→LUMO+7	6%
			HOMO-3→LUMO+8	5%
3.393	365	0.017	HOMO-3→LUMO+9	73%
			HOMO-6→LUMO+1	6%
4.383	283	0.018	HOMO-15→LUMO+3	86%

[Ta₆Br₁₂(H₂O)₄trans-(OH)₂]

Electronic excitation energy (eV)	λ (nm)	<i>f</i>	Nature	
1.821	681	0.016	HOMO→LUMO	87%
2.013	616	0.013	HOMO→LUMO+4	72%
			HOMO-1→LUMO	8%
			HOMO-1→LUMO+3	7%
2.020	614	0.015	HOMO→LUMO+5	72%
			HOMO-2→LUMO	11%
2.254	550	0.007	HOMO-1→LUMO+3	76%
			HOMO-3→LUMO+3	6%
2.681	462	0.034	HOMO-4→LUMO+1	28%
			HOMO-5→LUMO+2	17%
			HOMO-3→LUMO+2	7%
			HOMO-6→LUMO+6	6%
3.084	402	0.012	HOMO-6→LUMO+6	38%
			HOMO-3→LUMO+8	10%
			HOMO-6→LUMO+7	8%
			HOMO-4→LUMO+7	6%
3.113		0.019	HOMO-6→LUMO+2	19%
			HOMO-4→LUMO+4	15%
			HOMO-2→LUMO+10	14%
			HOMO-2→LUMO+9	10%
			HOMO-3→LUMO+8	10%
3.151		0.011	HOMO-2→LUMO+10	63%
			HOMO-6→LUMO+6	8%
			HOMO-4→LUMO+7	6%

3.208	0.022	HOMO-3→LUMO+9 HOMO-6→LUMO+1	73% 6%
3.510	0.012	HOMO-5→LUMO+10 HOMO-8→LUMO+1 HOMO-4→LUMO+11	61% 17% 9%
3.685	0.001	HOMO-5→LUMO+10 HOMO-8→LUMO+1 HOMO-4→LUMO+11	61% 17% 9%

References

- a) A. Renaud, M. Wilmet, T. G. Truong, M. Seze, P. Lemoine, N. Dumait, W. Chen, N. Saito, T. Ohsawa, T. Uchikoshi, N. Ohashi, S. Cordier and F. Grasset, *J. Mater. Chem. C*, 2017, **5**, 8160-8168. b) W. Koknat, J. A. Parsons and A. Vongvusharintra, *Inorg. Chem.*, 1974, **13**, 1699-1702. c) J. L. Meyer and R. E. McCarley, *Inorg. Chem.*, 1978, **17**, 1867-1872.
- D. N. T. Hay and L. Messerle, *J. Struct. Biology*, 2002, **139**, 147-151.
- M. N. Sokolov, P. A. Abramov, M. A. Mikhailov, E. V. Peresypkina, A. V. Virovets and V. P. Fedin, *Z. Anorg. Allg. Chem.*, 2010, **636**, 1543-1548
- a) J. Rodriguez-Carvajal, *Physica B*, 1993, **192**, 55-69. b) T. Roisnel and J. Rodriguez-Carvajal, *Epdic 7: European Powder Diffraction, Pts 1 and 2*, 2001, **378-3**, 118-123.
- a) F. Fonseca Guerra, J. G. Snijders, G. te Velde and E. J. Baerends, *Theo. Chem. Acc.*, 1998, **99**, 391-403. b) G. te Velde, F. M. Bickelhaupt, E. J. Baerends, C. Fonseca Guerra, S. J. A. van Gisbergen, J. G. Snijders and T. Ziegler, *J. Comput. Chem.*, 2001, **22**, 931-967. c) *Amsterdam Density Functional (ADF)*, 2016.01; SCM, Theoretical Chemistry, Vrije Universiteit: Amsterdam, The Netherlands, 2016.
- Y. K. Zhang and W. T. Yang, *Physical Review Letters*, 1998, **80**, 890-890.
- H. Vosko, L. Wilk and M. Nusair, *Can. J. Phys.*, 1980, **58**, 1200-1211.
- a) van Lenthe, A. Ehlers and E. J. Baerends, *J. Chem. Phys.*, 1999, **110**, 8943-8953. b) van Lenthe and E. J. Baerends, *J. Comput. Chem.*, 2003, **24**, 1142-1156.
- a) K. Costuas, A. Garreau, A. Bulou, B. Fontaine, J. Cuny, R. Gautier, M. Mortier, Y. Molard, J. L. Duvail, E. Faulques and S. Cordier, *Phys. Chem. Chem. Phys.*, 2015, **17**, 28574-28585. b) M. Kepenekian, Y. Molard, K. Costuas, P. Lemoine, R. Gautier, A. G. Soraya, B. Fabre, P. Turban and S. Cordier, *Mater. Horiz.*, 2019, **6**, 1828-1833.
- S. Grimme, S. Ehrlich and L. Goerigk, *J. Comput. Chem.*, 2011, **32**, 1456-1465.
- C. C. Pye and T. Ziegler, *Theo. Chem. Acc.*, 1999, **101**, 396-408.